Full-Wave Segmentation Analysis of Arbitrarily Shaped Planar Circuit

Shih-Ping Liu, *Student Member, IEEE,* and Ching-Kuang C. Tzuang, *Senior Member, IEEE*

***Abstract*—This paper presents a novel full-wave segmentation method for analyzing a complex and large microwave planar circuit which is divided into several smaller segments with corresponding multiport network parameters. They are obtained by a full-wave space-domain integral-equation technique in connection to a proposed excitation model based on the equivalence principle. The integral equation is solved numerically by Galerkin's procedure resulting in the generalized scattering-matrix (GSM) descriptions of all the subcircuit segments. The combination of these GSM's yields an overall network characterization of the composite circuit. Rigorous convergence studies and extensive validity checks confirm the reliability and accuracy of the proposed method. The novel technique immediately demonstrates its obvious application for quantitative characterization of higher order modes associated with a microwave-circuit discontinuity problem. Finally, very good agreement is obtained in a comparative study of an arbitrary planar structure analyzed by our full-wave method with and without segmentation, respectively.**

***Index Terms*— Equivalence principle, equivalent source excitation, full-wave segmentation method, generalized scattering matrix (GSM), higher order modes, multimode, near discontinuity de-embedding, space-domain integral equation.**

I. Introduction

THE segmentation method has been extensively developed in the past for the analyses of two-dimensional (2-D) planar microwave circuits [1]–[3]. Sorrentino and his coworkers extended this method to solve three-dimensional (3-D) electromagnetic (EM) problems such as waveguide circuits [4], [5], via-hole grounds in microstrip [6], and coplanar waveguide (CPW) discontinuity problem [7], and further to develop an efficient optimization tool for the design of waveguide components [8], [9]. The segmentation method applies the concept of subdividing a microwave circuit into several smaller portions called segments and analyzes these segments individually by field-theoretic means such as the planar-circuit approach (PCA) [1]–[3] and mode-matching (MM) method [4]–[7]. To facilitate the tangential fields matching along the interfaces between all the segments to obtain a complete solution of the entire microwave-circuit, equivalent network representations of the segments in terms of S (scattering) [1], Z (impedance) [2], [3], and Y (admittance) [4]–[7] matrices allow analysis of the complicated microwave circuit by linear network manipulation.

Manuscript received April 23, 1996; revised May 19, 1997. This work was supported in part by the National Science Council, Taiwan, R.O.C., under Grant NSC84-2622-E009-011.

The authors are with the Institute of Electrical Communication Engineering, National Chiao Tung University, Hsinchu, Taiwan, R.O.C.

Publisher Item Identifier S 0018-9480(97)06058-4.

The full-wave segmentation method published in open literature applied the MM technique by properly dividing a 3-D passive microwave component into typical well-known waveguide sections [4]–[7]. Strictly speaking, the conventional MM method applied to the cascaded step discontinuity problems of the microstrip [10], [11] and the finline [12] also belongs to the segmentation technique since it combines the solutions for the cascaded junctions and the interconnecting line section between them—however, using the generalized scattering matrix (GSM). Here we propose an alternative full-wave segmentation approach to solve a planar circuit of complicated geometry. We invoke the space-domain integral-equation technique to solve individual smaller segments and then obtain the equivalent multiport network model for each segment using the GSM representation, from which the network parameters of the entire microwave circuit are a direct result of combining all the GSM's.

The full-wave segmentation method presented here has the following advantages.

1) The segmentation of a complicated microwave circuit has, in general, no limitation to the geometry of the circuit, while the EM fields over the interface planes between adjacent segments can be precisely defined. This makes the method very flexible and versatile.
2) Adoption of the GSM representation for the solution obtained by the present method facilitates quantitative analysis of higher order modes or multimodes without the need to know their characteristic impedance. Furthermore, the reference plane for extracting the scattering parameters can be arbitrarily defined unlike the discontinuity junction in the conventional MM method. Thus, much fewer normal modes are required in our technique than the MM method, resulting in much less numerical effort in evaluating the additional modes.
3) The method is especially suitable for analyzing a complicated and large microwave circuit. Each segment of the circuit in the segmentation procedure is solved individually with less memory storage, which overcomes a memory problem in solving a large microwave circuit, and less central processing unit (CPU) time in particular. Total computational time for all individual segments is considerably reduced according to our extensive numerical studies, when compared with the CPU time needed for analyzing the entire circuit as a whole. In many circumstances, only one or a few segments in a microwave circuit need modification when tuning or optimizing the circuit without resorting to changing all

0018–9480/97$10.00 © 1997 IEEE

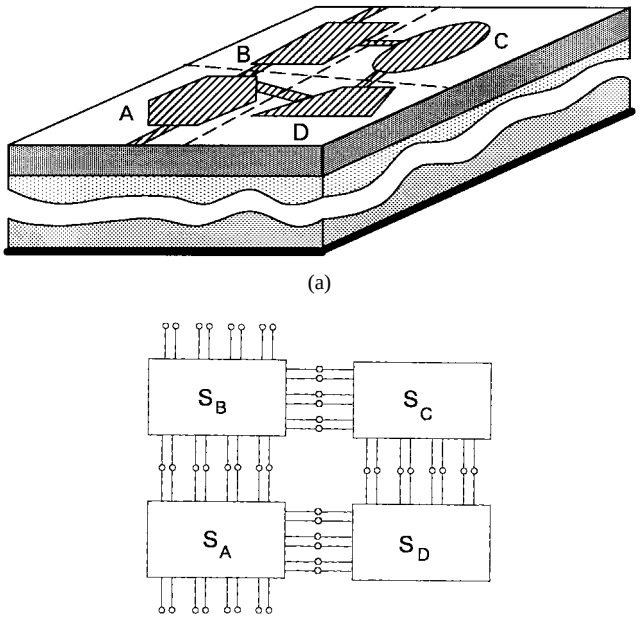

Fig. 1. (a) An arbitrarily shaped printed planar circuit to be analyzed by the proposed full-wave segmentation method and (b) the equivalent segmented multiport GSM model.

the segmented networks. When this is the case, we only need to iteratively obtain the new GSM's of these fewer segments, and then evaluate the overall circuit performance by combining the new GSM's with the previously saved GSM's of the unaltered segments. This makes our method very appealing as part of an efficient full-wave EM optimization tool.

Section II-A will describe a model that enables us to extract the GSM representation of an arbitrarily shaped microwave discontinuity problem. A space-domain integral equation for the equivalent model is derived by using the reciprocity theorem and the equivalence principle, and is solved subsequently by Galerkin's procedure of the moment method. These will be presented in Section II-B. An extensive convergence study for a particular circuit is reported in Section III-A to examine the accuracy and reliability of the novel full-wave segmentation technique. A comparison of our theoretical results with other available results for the same circuit is shown in Section III-B, which also illustrates the quantitative behavior of higher order modes excited near the discontinuity of the circuit. Section III-C further reports a self-explanatory result to validate the present method. Finally, in Section IV, the numerical results of applying the full-wave segmentation technique to a complex structure are presented to demonstrate the usefulness and potential of the proposed method. A discussion about the novel segmentation method is given in Section V.

II. Model and GSM Space-Domain Integral-Equation Method

In this paper, we attempt to develop a full-wave segmentation approach to accurately and efficiently investigate a complicated microwave planar circuit. Undoubtedly, one may be inclined to directly analyze the entire circuit without knowing the merits of the segmentation approach. Fig. 1 pictorially illustrates the proposed segmentation model. Assuming that a planar microwave circuit of arbitrary shape is printed on a system of stratified substrates [Fig. 1(a)], one may divide the printed circuit into, say, four smaller segments denoted as blocks A, B, C, and D, respectively. Two external ports are connected to blocks A and B, respectively. The interconnections between various segments can be uniform transmission lines in the form of microstrip or multiple coupled microstrips. Four additional reference planes are placed across the interconnecting lines between the adjacent blocks to define the input or output ports for the respective segments. The coupling between diagonal blocks $A(B)$ and $C(D)$ is assumed negligible. The EM fields in the individual segments can be uniquely determined by knowledge of the tangential electric (or magnetic) fields over the corresponding reference planes. Therefore, using the equivalence principle [13], we characterize each segment by the integral-equation technique as a multiport network, as shown in Fig. 1(b), in terms of GSM representation. At the interface plane between any two blocks, Fig. 1(b) illustrates multiple electric ports in terms of modes rather than the physical interconnection line(s).

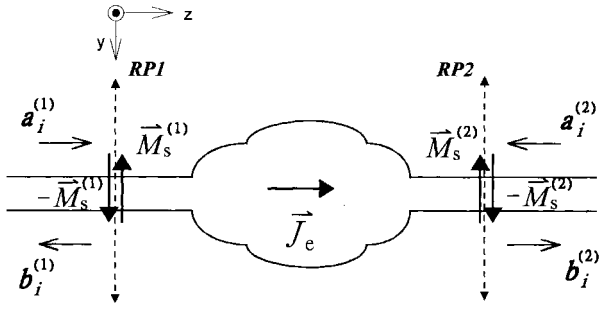

Fig. 2. Equivalent magnetic-current sources as the excitation model for a physical two-port discontinuity problem.

A. Equivalent Source Excitation of a Segmented Circuit

Fig. 2 depicts the fundamental underlying concept of the equivalent EM model of a certain smaller segment of Fig. 1. For convenience of illustration, we use a typical two-port circuit as an example of the segment. Applying the equivalence principle [13], we place two fictitious electric walls at the reference planes $RP1$ and $RP2$, respectively; equivalent magnetic-current sources $\vec{M}_s^{(1)}$ and $\vec{M}_s^{(2)}$ are, therefore, imposed on the respective walls to retain the original EM field of the structure. The current sources are directly related to the incident waves and reflected waves, which are both represented in terms of normal modes on the interconnecting lines. They are given as

$$\vec{M}_s^{(1)} = -\hat{u}_z \times \vec{E}_t^{(1)}|_{RP1} = -\hat{u}_z \times \sum_{i=1}^{M1} (a_i^{(1)} + b_i^{(1)}) \vec{e}_i^{(1)} \quad (1)$$

$$\vec{M}_s^{(2)} = \hat{u}_z \times \vec{E}_t^{(2)}|_{RP2} = \hat{u}_z \times \sum_{i=1}^{M2} (a_i^{(2)} + b_i^{(2)}) \vec{e}_i^{(2)} \quad (2)$$

where the superscripts (1) and (2) denote the reference planes at physical port one and port two, respectively; $\vec{e}_i^{(\nu)}$ is the normalized transverse vector electric field of the ith mode; $a_i^{(\nu)}$

and $b_i^{(\nu)}$ are the complex amplitude coefficients of the ith mode incident on, and scattered from, physical port ν, respectively, $(\nu = 1, 2)$. Each physical port ν supports electrically multiple ports for modes $i = 1$ to $M\nu$ as illustrated in Fig. 1(b). The expansion number of modes $M\nu$, in theory, should be infinite to represent the total transverse electric field $\vec{E}_t^{(\nu)}$ at the reference plane. However, in practice, we apply the first few dominant and higher order modes to approximate the total field. This assumption is valid so long as the reference plane is not very close to the discontinuity. Note that the equivalent sources also serve as an excitation mechanism for the discontinuity problem in our method. Besides the antenna and scattering problems, a similar concept of applying the equivalence principle was also reported elsewhere in the literature [5], [6], [14], [15].

Careful manipulations of (1) and (2) should be exercised for obtaining accurate scattering parameters provided the surface waves [16], EM radiation [17], or leaky modes [18] are excited at discontinuities. However, the discontinuity problems or models defined in the paper do not exhibit the above-mentioned leakage phenomena since the test circuits are placed in a rectangular waveguide tube.

B. GSM Space-Domain Integral Equation

Let a testing current $\vec{J}_t$ be applied on the location where the arbitrarily shaped conducting strips reside, as shown in Fig. 2. The resultant electric and magnetic fields are denoted by $\vec{E}_{tt}$ and $\vec{H}_{tt}$, respectively. On the other hand, an induced surface current $\vec{J}_e$ on the conducting strips caused by the impressed sources $\vec{M}_s^{(1)}$ and $\vec{M}_s^{(2)}$ helps contribute the total electric field $\vec{E}_s$ that vanishes on the conducting strips. Applying the reciprocity theorem [13], [15], the reaction relation for the two sets of sources $(\vec{M}_s^{(1)}, \vec{M}_s^{(2)}, \vec{J}_e)$ and $\vec{J}_t$ becomes

$$\iiint_{\nu} \vec{E}_s \cdot \vec{J}_t \, d\tau = \iiint_{\nu} [\vec{E}_{tt} \cdot \vec{J}_e - \vec{H}_{tt} \cdot (\vec{M}_s^{(1)} + \vec{M}_s^{(2)})] \, d\tau. \quad (3)$$

Since the total tangential electric field on the conducting strips must be zero, the left-hand side (LHS) of (3) vanishes. Simplifying (3), we obtain

$$\iint_{\text{strip}} \vec{E}_{tt} \cdot \vec{J}_e \, ds = \iint_{S_1} \vec{H}_{tt} \cdot \vec{M}_s^{(1)} \, ds + \iint_{S_2} \vec{H}_{tt} \cdot \vec{M}_s^{(2)} \, ds \quad (4)$$

where S_n $(n = 1, 2)$ is the cross section at physical port n. Note that referring to Fig. 2, one may wish to place magnetic walls at the reference planes instead of electric walls, and two sheets of electric currents are imposed over the walls to set up an alternative equivalent problem to Fig. 2 [13]. The electric $(\vec{E}_{tt})$ and magnetic $(\vec{H}_{tt})$ fields in (4) can be obtained by the principle of superposition when the dyadic Green's functions of the boundary-value problem are known. Using (4) and applying the reciprocity property of the dyadic Green's function, one may also derive the well-known integral-equation formulation reported by Jansen (see the Appendix).

The excited surface current distribution $\vec{J}_e$ can be expanded by the conventional rooftop bases denoted by

$$\vec{J}_e = \sum_{j=1}^{Ny} I_{y,j} J_{y,j}(y,z)\hat{u}_y + \sum_{j=1}^{Nz} I_{z,j} J_{z,j}(y,z)\hat{u}_z \quad (5)$$

where $I_{y,j}$ and $I_{z,j}$ are unknown current coefficients of the rooftop expansion functions $J_{y,j}$ and $J_{z,j}$, respectively, and Ny and Nz are the total numbers of the rooftop bases. Substituting (1), (2), and (5) into (4), and applying the Galerkin's procedure where the testing current $\vec{J}_t$ is in sequence identical to each of the bases that expand the current $\vec{J}_e$, we may express the unknown current expansion coefficients in terms of the unknown modal amplitudes ($a_i^{(1)}$, $a_i^{(2)}$, $b_i^{(1)}$, and $b_i^{(2)}$) at both physical port one and port two as follows:

$$[B^{(1)}]([\boldsymbol{a}^{(1)}] + [\boldsymbol{b}^{(1)}]) - [B^{(2)}]([\boldsymbol{a}^{(2)}] + [\boldsymbol{b}^{(2)}]) = \begin{bmatrix} A_{yy} & A_{zy} \\ A_{yz} & A_{zz} \end{bmatrix} \begin{bmatrix} I_{ey} \\ I_{ez} \end{bmatrix} = [A][I_e] \quad (6)$$

where $[\boldsymbol{a}^{(\nu)}]$ and $[\boldsymbol{b}^{(\nu)}]$ are column vectors with elements of the unknown complex modal amplitudes $a_i^{(\nu)}$ and $b_i^{(\nu)}$, respectively, for $i = 1, 2, \cdots, M\nu$ and $\nu = 1$ or 2. Column vectors $[I_{ey}]$ and $[I_{ez}]$ consist of the unknown current coefficients $I_{y,j}$ and $I_{z,j}$, respectively. The elements of other matrices are given by

$$(A_{pq})_{ij} = \iint_{\text{strip}} E_p(J_{eq,i}\hat{u}_q) J_{ep,j} \, ds \qquad p, q \in \{y, z\} \quad (7a)$$

$$(B^{(\nu)})_{ij} = \iint_{S_\nu} \vec{H}(J_{ey,i}\hat{u}_y) \times \vec{e}_j^{(\nu)} \, ds \quad (7b)$$

$$(B^{(\nu)})_{i+Ny,j} = \iint_{S_\nu} \vec{H}(J_{ez,i}\hat{u}_z) \times \vec{e}_j^{(\nu)} \, ds \qquad \nu = 1 \text{ or } 2 \quad (7c)$$

where $E_p(J_{eq,i}\hat{u}_q)$ is defined as the p component of the electric field arising from the current source $J_{eq,i}\hat{u}_q$, and similar definitions are for $\vec{H}(J_{ey,i}\hat{u}_y)$ and $\vec{H}(J_{ez,i}\hat{u}_z)$. Finally, we impose the continuous tangential magnetic fields at the reference planes $RP1$ and $RP2$, respectively, yielding the following two equations:

$$\sum_{j=1}^{N1} (a_j^{(1)} - b_j^{(1)}) \vec{h}_j^{(1)} = \vec{H}(\vec{M}_s^{(1)}) + \vec{H}(\vec{M}_s^{(2)}) + \vec{H}(\vec{J}_e), \qquad \text{at the plane RP1} \quad (8)$$

$$\sum_{j=1}^{N2} (-a_j^{(2)} + b_j^{(2)}) \vec{h}_j^{(2)} = \vec{H}(\vec{M}_s^{(1)}) + \vec{H}(\vec{M}_s^{(2)}) + \vec{H}(\vec{J}_e), \qquad \text{at the plane RP2} \quad (9)$$

where $\vec{H}(\vec{M}_s^{(1)})$, $\vec{H}(\vec{M}_s^{(2)})$, and $\vec{H}(\vec{J}_e)$ represent the magnetic fields caused by the magnetic or electric current sources of their respective arguments. Next, we take the inner products of (8) and (9) with the known transverse modal fields $\vec{e}_m^{(1)}$ for

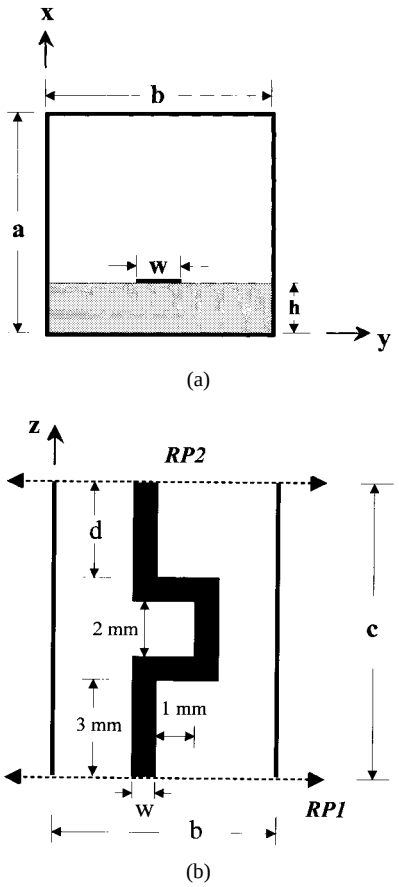

Fig. 3. A shielded asymmetric meander microstrip structure for validating the proposed full-wave segmentation method. (a) Cross section of the shielded microstrip. (b) Asymmetric meander line. $\varepsilon_r = 10.2, h = 0.635$ mm, $w = 0.6$ mm, $a = 11$ h, $b = 6$ mm, and $d = 3$ mm.

$m = 1, \cdots, N1$ and $\vec{e}_n^{(2)}$ for $n = 1, \cdots, N2$, receptively, over the corresponding cross sections, leading to

$$[\boldsymbol{a}^{(1)}] - [\boldsymbol{b}^{(1)}] = [P_1]([\boldsymbol{a}^{(1)}] + [\boldsymbol{b}^{(1)}]) - [Q_1]([\boldsymbol{a}^{(2)}] + [\boldsymbol{b}^{(2)}]) + [B^{(1)}]^t[I_e] \quad (10)$$

$$-[\boldsymbol{a}^{(2)}] + [\boldsymbol{b}^{(2)}] = [P_2]([\boldsymbol{a}^{(1)}] + [\boldsymbol{b}^{(1)}]) - [Q_2]([\boldsymbol{a}^{(2)}] + [\boldsymbol{b}^{(2)}]) + [B^{(2)}]^t[I_e] \quad (11)$$

where the superscript t represents a matrix transpose operation and

$$(P_\nu)_{ij} = \iint_{S_\nu} \vec{e}_i^{(\nu)} \times \vec{H}(\vec{e}_j^{(1)})\, ds \quad (12a)$$

$$(Q_\nu)_{ij} = \iint_{S_\nu} \vec{e}_i^{(\nu)} \times \vec{H}(\vec{e}_j^{(2)})\, ds, \qquad \nu = 1 \text{ or } 2. \quad (12b)$$

$\vec{H}(\vec{e}_j^{(1)})$ and $\vec{H}(\vec{e}_j^{(2)})$ are the magnetic fields arising from the magnetic sources with the same distribution as $\vec{e}_j^{(1)}$ and $\vec{e}_j^{(2)}$, respectively. The inner product satisfies the modal orthogonality given as

$$\iint_{S_\nu} \vec{e}_i^{(\nu)} \times \vec{h}_j^{(\nu)} \cdot \hat{z}\, ds = \delta_{ij} \quad (13)$$

where δ_{ij} is the Kronecker delta function.

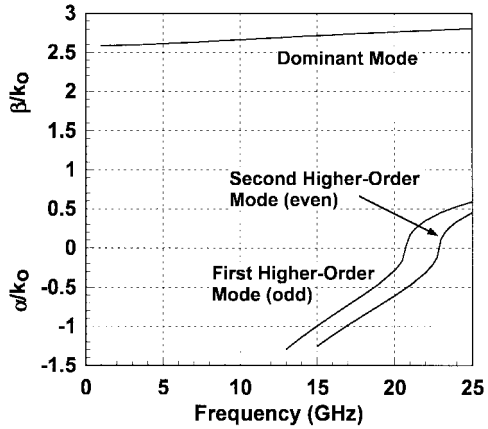

Fig. 4. Dispersion curves of the microstrip line in Fig. 3(a).

Making use of (10), (11), and (6), and eliminating the unknown vector of $[I_e]$, we can obtain the GSM from the following:

$$\begin{bmatrix} \boldsymbol{b}^{(1)} \\ \boldsymbol{b}^{(2)} \end{bmatrix} = ([I] + [Z])^{-1}([I] - [Z]) \begin{bmatrix} \boldsymbol{a}^{(1)} \\ \boldsymbol{b}^{(2)} \end{bmatrix} = \begin{bmatrix} S_{11} & S_{12} \\ S_{21} & S_{22} \end{bmatrix} \begin{bmatrix} \boldsymbol{a}^{(1)} \\ \boldsymbol{a}^{(2)} \end{bmatrix} \quad (14)$$

with

$$[Z_{11}] = [P_1] + [B^{(1)}]^t[A]^{-1}[B^{(1)}] \quad (15a)$$

$$[Z_{12}] = -[Q_1] - [B^{(1)}]^t[A]^{-1}[B^{(2)}] \quad (15b)$$

$$[Z_{21}] = -[P_2] - [B^{(2)}]^t[A]^{-1}[B^{(1)}] \quad (15c)$$

$$[Z_{22}] = [Q_2] + [B^{(2)}]^t[A]^{-1}[B^{(2)}] \quad (15d)$$

and $[I]$ is the identity matrix. Each partition S_{ij} is a submatrix, where every element S_{ij} (m, n) represents the scattering parameter of the mth mode scattered at physical port i for the nth mode incident on physical port j. Finally, the overall generalized scattering parameters of the composite planar circuit of Fig. 1, with respect to the two physical external ports, are readily obtained by combining the four GSM's computed using (14) and (15). The present method is versatile in that it can be reduced to solve physical one-port circuits or extended for physical multiport circuits. When a great number of basis functions are needed in analyzing a large printed circuit, most CPU time is spent calculating the elements of matrix $[A]_{N\times N}$ [(6) and (7)]. If the circuit is divided into n segments, then the total CPU time requirement will be reduced approximately by a factor n, showing one of the advantages of the method in efficiency.

III. Numerical Results

Before entering the segmentation procedure for analyzing a complicated planar circuit, we have to validate the developed method. Here, a simple shielded microstrip structure of an approximately 50-Ω meander line with its cross-sectional view and top view shown in Fig. 3(a) and (b), respectively, is investigated. This structure is clearly asymmetric. Fig. 4 plots the dispersion characteristics of the boxed 50-Ω uniform microstrip line. There are three modes plotted in Fig. 4. The

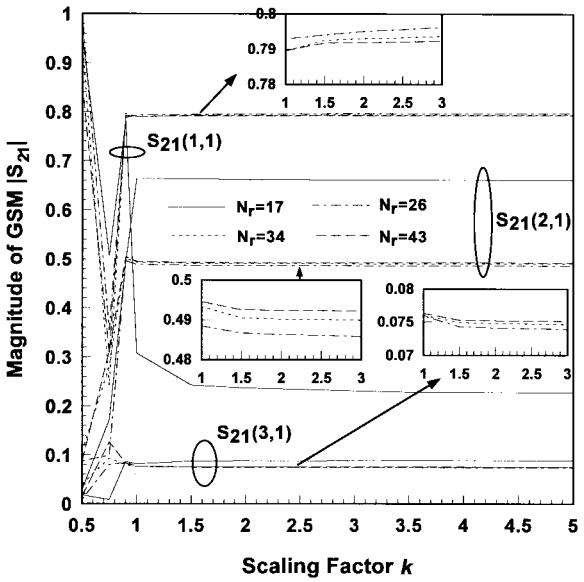

Fig. 5. Convergence study for the GSM values over the scaling factor k with the discretization resolution Nr as a controlling parameter.

dominant mode and the second higher order mode are in even symmetry, whereas the first higher order mode is in odd symmetry. We will use only three modes to approximate the total fields at both reference planes $RP1$ and $RP2$ [Fig. 3(b)]. The truncated values of $M1$ and $M2$ in (1) and (2), equal to three, reflect the assumption that all the rest of the higher order modes generated in the discontinuity problem have negligible contribution to the total fields at the reference planes.

A. Convergence Study for a Partial Segmented Printed Circuit

The dyadic Green's functions are introduced in (7) and (12) to derive the electric and magnetic fields. The Green's functions for the shielded structure of Fig. 3 can be represented by double infinite sums of the Fourier series [15], where the summation terms (spectral terms) must be truncated in practice. Ideally, on the other hand, the numbers of the rooftop bases Ny and Nz in (5) have to also be infinite. Thus, it is necessary to study the convergence property of the GSM against the numbers of the Fourier series and the rooftop bases simultaneously. To this end, we define a resolution factor Nr as the number of subsections per guided-wave wavelength for circuit discretization. In the process of gridding, we assume the mesh is a square. Therefore, the mesh has dimension Δy equal to Δz, or the ratio of the dominant mode's guided wavelength λg to the resolution factor Nr. The numbers of the double summation terms in computing the dyadic Green's functions are expressed as $k \times b/\Delta y$ and $k \times c/\Delta z$, where k is a scaling factor and has been investigated elsewhere [15], [19].

With these notations, Fig. 5 shows the convergence properties of the computed transmission coefficients $S_{21}(m,n)$ at 21 GHz using Nr and k as controlling parameters. For any given value of the resolution factor Nr, the values of $S_{21}(1,1)$, $S_{21}(2,1)$, and $S_{21}(3,1)$ converge quickly after k greater than 1.5. Increasing the value of k means the number of spectral terms is increased. On the other hand, the magnitudes of the scattering parameters $|S_{21}|$ converge to almost the same values within 0.6% when the number of bases Nr per wavelength is greater than 34 while the value of k is greater than 2. The results shown in Fig. 5 manifest the absolute convergence property in our formulation in the same manner reported earlier for the study of waveguide and scattering problems, where the converged solutions were obtained by a sufficiently large number of satisfactory basis functions coupled with a large inner-product truncation point [20]. Therefore, in the following computations of GSM's, we are confident of applying $k = 2$ and $Nr = 34$ for the converged and correct solutions.

B. Validity Check Against the Spectral-Domain Approach Program

We continue validating the present method by comparing our results with those obtained from the LINMIC+ package[1] which employs the SDA [spectral-domain approach (SDA)] for the same circuit of Fig. 3. Fig. 6(a) and (b) plots and compares the magnitude and phase of the scattering parameters, respectively. Very good agreement is obtained for both methods. Only slight deviation in magnitude is observed throughout the wide frequency span below 20 GHz while the phase agrees excellently. Notice that the simulated environments for our method and LINMIC are different in that the former assumes two semi-infinite long microstrip lines enclosed by the rectangular shielding of Fig. 3(a), whereas the latter assumes a fully enclosed electric box. The former allows the higher order modes to either decay or propagate outside the reference planes. We speculate this is the reason for the small discrepancy in the S-parameter's magnitude.

We next focus our attention on the data between 20 and 25 GHz in Fig. 6, where the first two higher order modes become influential. Referring to Fig. 4, we realize that the cutoff frequencies of the first two higher order modes are located at approximately 20.7 and 22.9 GHz, respectively. The meander line under analysis is *asymmetric*, resulting in simultaneous excitation of these two higher order modes with considerable amount at higher frequencies. Not surprisingly, the transmission parameters $S_{21}(2,1)$ and $S_{21}(3,1)$ extracted from the GSM show peak values approximately at the threshold frequencies. The first (second) higher order odd (even) mode transmitted from the reference plane $RP2$ has about -7 dB (-11 dB) in magnitude at the cutoff frequency. These values are significant, resulting in a noticeable impact on the $S_{21}(1,1)$ at higher frequencies where our results start to depart from the LINMIC's results.

The power conservation and the reciprocity condition associated with the GSM of the particular problem of Fig. 3 are investigated. The reciprocal network mandates the GSM is symmetric. The assumed loss-free problem requires that in each column of the GSM, the sum of the squares of the elements corresponding to the scattered *propagating* modes due to an incident *propagating* mode must be equal to unity [21]. This is expressed by

$$\sum_{p}(|S_{ij}(p,q)|^2+|S_{jj}(p,q)|^2=1, \qquad i,j=1\text{or}2\,(i\neq j) \quad (16)$$

[1] LINMIC+/N, Jansen Microwave, Ratingen, Germany.

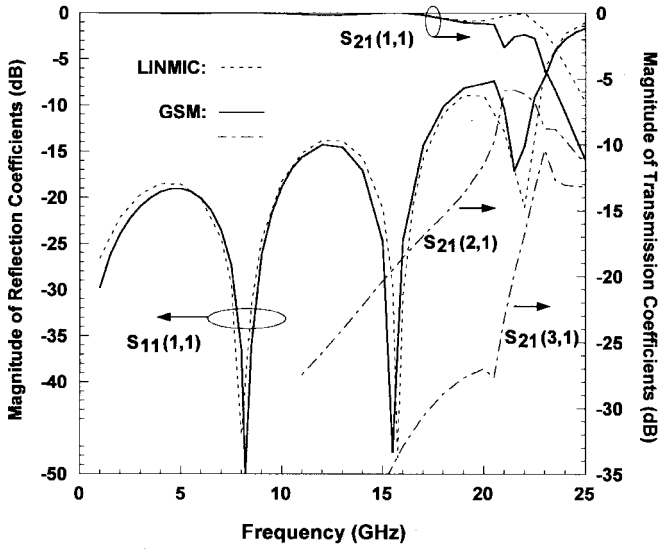

(a)

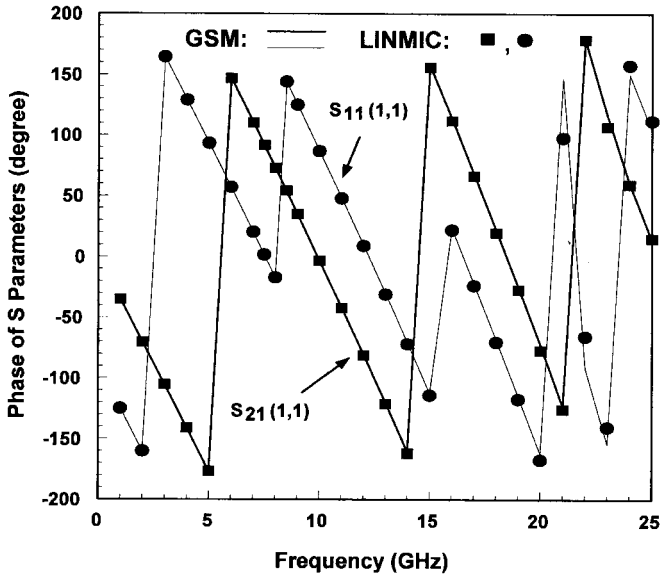

(b)

Fig. 6. Comparisons of the S-parameters obtained by the present method and by LINMIC. (a) Magnitude of the scattered dominant mode and the transmission parameters of the first two higher order modes at higher frequencies. (b) Phase of the scattered dominant mode.

where p *and* q are the indexes for the scattered and the incident *propagating* modes, respectively. Careful numerical studies show that the computed GSM's are indeed reciprocal and satisfy (16). We also analyze a variety of *symmetric* planar structures such as the cascaded microstrip step discontinuities and coupled microstrips-to-microstrip transition using the present method. Assuming that one propagating even/odd mode is incident on any physical port, we find no generation of the odd/even modes, whether above or below cutoff. This agrees with our physical expectation.

C. Shifting Reference Plane for Near-Discontinuity Characterization

By shifting the reference plane $RP2$ gradually away from the discontinuity while fixing the position of plane $RP1$ and

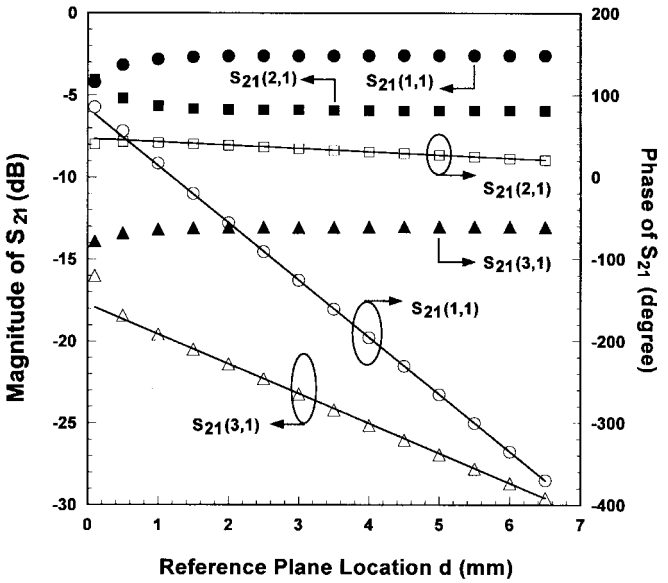

Fig. 7. Comparison of the transmission parameters of the calculated GSM (indicated by various symbols) at different reference planes and three predicted straight lines directly obtained from the dispersion curves of Fig. 4.

computing the GSM of Fig. 3 at 21 GHz, the magnitude and phase of the transmission parameters at the physical port two for all three modes are plotted in Fig. 7 with three sets of symbols, against the distance d measured right from the discontinuity. The three modes include two propagating modes and one evanescent mode at 21 GHz. When $RP2$ moves, as seen in Fig. 7, the transmitted propagating modes, $S_{21}(1,1)$ and $S_{21}(2,1)$, should maintain their field magnitudes and experience phase delays only. In contrast, the transmitted evanescent mode $S_{21}(3,1)$ should preserve its phase rather than magnitude. Fig. 7 also plots three straight lines drawn from the location of the discontinuity with slopes directly evaluated from the corresponding propagation constants of Fig. 4. For the two propagating modes, the slopes $(-\beta \times 180/\pi)$ are $-69.9°/-4.1°$/mm, respectively. For the evanescent mode, the line with slope $(-\alpha \times 8.686)$ of -1.82 dB/mm is obtained. These three lines coincide with the computed GSM data very well. As a result, the data obtained from the GSM show great agreement with the predicted data from the dispersion characteristics of the various modes. It is noted that larger discrepancy will occur when d approaches zero for the three straight lines, and hence, more normal modes are required in the formulation to obtain accurate solutions. On the other hand, in this particular case, three modes are sufficient to approximate the transverse fields as d is 1 mm away from the discontinuity. According to the experience gained in a number of studies, the excited higher order evanescent modes of magnitude below -25 dB at the reference planes may negligibly influence the computed GSM of lower order modes.

IV. Full-Wave Segmentation Applied with GSM Space-Domain Integral-Equation Method

In the previous section we learn that the GSM space-domain integral-equation method is a powerful approach for obtaining the GSM network representation of arbitrarily shaped segment,

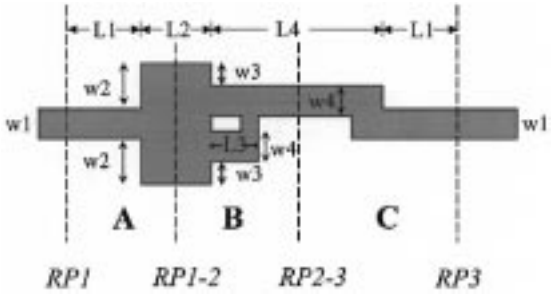

Fig. 8. Example of a complex circuit structure, which is unintentionally divided into three segments for the full-wave segmentation method. Various widths and lengths of the circuit are $w_1 = w_2 = 0.6$ mm, $w_3 = 0.3$ mm, $w_4 = 0.45$ mm, $L_1 = 1.2$ mm, $L_2 = 1.8$ mm, $L_3 = 0.9$ mm, and $L_4 = 3.3$ mm.

in contrast to the conventional PCA and the MM segmentation method requiring regular shapes. By means of direct algebraic manipulation of the GSM's of various segments according to the interconnection lines between the segments [10], [12], the complete GSM representation of the whole network can be obtained by spending almost negligible CPU time. While manipulating the GSM's algebraically, we are in effect matching the fields across the interfaces between the various segments in a network sense. Fig. 8 shows a test example to illustrate how the full-wave segmentation technique proceeds. It consists of a 50-Ω microstrip line with an enlarged step discontinuity followed by coupled microstrip lines, and combined to form the output port with two bends. This complex two-port printed circuit is placed in a waveguide tube as shown in Fig. 3(a).

Fig. 8 depicts how we unintentionally divide the structure into three segments in cascade. Totally, there are four reference planes in Fig. 8, namely, $RP1$, $RP1-2$, $RP2-3$, and $RP3$. In view of the results shown in Figs. 6 and 7, we apply the GSM space-domain integral-equation method to obtain the GSM's of the three segments using three modes within the frequency band up to 17 GHz. Since the segments are in cascade configuration, the overall scattering parameters can be obtained by sequentially combining two GSM's. The new GSM after combining segment A and segment B (Fig. 8) can be derived using a straightforward procedure [10] and given by [12]

$$S_{11} = S_{11}^A + S_{12}^A S_{11}^B Y S_{21}^A \tag{17a}$$
$$S_{12} = S_{12}^A (I + S_{11}^B Y S_{22}^A) S_{12}^B \tag{17b}$$
$$S_{21} = S_{21}^B Y S_{21}^A \tag{17c}$$
$$S_{22} = S_{22}^B + S_{21}^B Y S_{22}^A S_{12}^B \tag{17d}$$

where

$$Y = (I - S_{22}^A S_{11}^B)^{-1} \tag{18}$$

and S_{ij}, S_{ij}^A, and S_{ij}^B for $i, j = 1$ or 2, are the submatrices of the new GSM and the old GSM's for segments A and B, respectively. Fig. 9(a) and (b) plot the magnitude and phase of the transmission and reflection coefficients of the dominant mode for the comparative studies of the full-wave segmentation method against the full-wave analysis of the entire network without segmentation. The two solutions almost coincide with each other without noticeable difference.

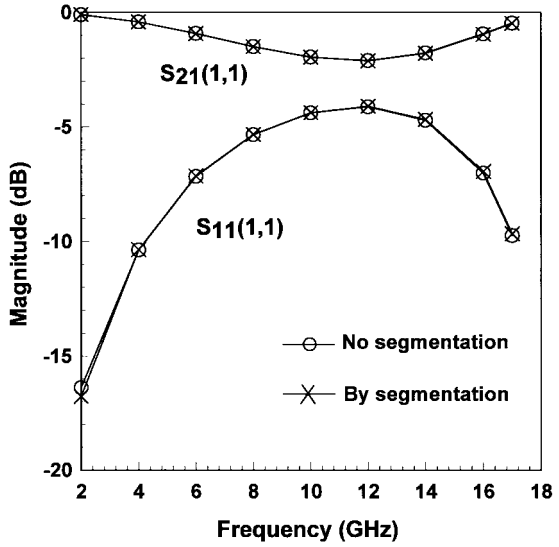

(a)

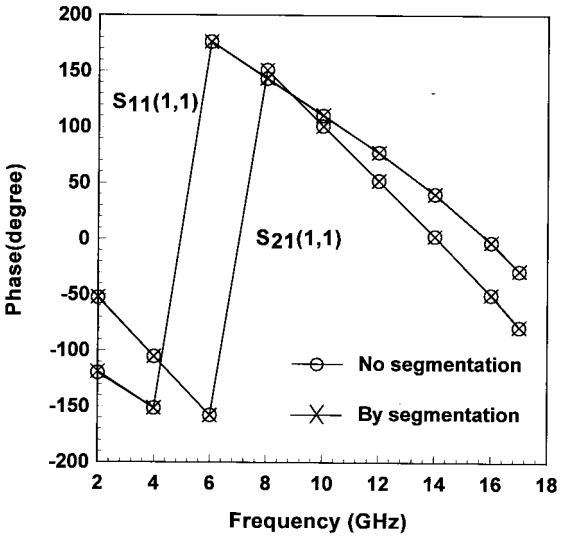

(b)

Fig. 9. Comparison of (a) the magnitude and (b) the phase of the GSM's obtained by analyzing the circuit of Fig. 8 with and without the segmentation approach.

Thus the three-mode approximation of the GSM is a good assumption in our test study and good tangential field matching by the network interface is achieved.

V. Conclusion

A novel full-wave segmentation method is presented, employing the full-wave space-domain integral equation for obtaining the GSM's of the various subcircuit segments, then followed by network matching the fields across the interfaces between the interconnected segments to form the complete network description of an arbitrarily shaped multiport printed circuit. The GSM space-domain integral equation is well suited for obtaining the GSM of any multilayered planar or quasi-planar printed circuit. A series of validity checks of the GSM space-domain integral equation confirms that all the data presented in this paper are converged and correct

solutions. The criterion for obtaining such converged solutions for the GSM is reported in Section III-A, while the results in Section III-C imply that only three modes are required to yield satisfactory network matching the fields between the various segments for the particular case study.

A printed-circuit test example of Fig. 8 is divided at random into three segments. The combined results of connecting the individual GSM's of each segment agree excellently with the scattering parameters obtained by analyzing the complete network without segmentation for the complex and large circuit. The proposed full-wave segmentation method demonstrates the following features, namely: 1) approximately 65% saving in CPU time for analyzing the structure of Fig. 8 with three segments as compared to that required for the whole circuit without segmentation; 2) estimated two-thirds in memory reduction for the same test case; and 3) the capability of near discontinuity de-embedding of higher order modes or multimodes. Furthermore, the efficiency of the segmentation method increases with the complexity and dimension of the circuit under analysis, as well as the number of segments.

Although the full-wave segmentation method using three-mode approximation works well for all the case studies reported here, it is highly possible that a great number of modes are needed to faithfully represent the transverse field across the segmentation plane between two subdivisions to obtain accurate scattering parameters. Consequently when the planar circuit contains strongly coupled subcircuits, one may exercise certain EM expertise to pick the location of division that avoids the region of strong coupling. Otherwise one has to significantly increase the number of modes.

APPENDIX

If magnetic walls and equivalent electric-current sheets are used in Fig. 2, (4) should be modified as

$$\iint_{\text{strip}} \vec{E}_{tt}\cdot\vec{J}_e\,ds = -\iint_{S_1}\vec{E}_{tt}\cdot\vec{J}_s^{(1)}\,ds - \iint_{S_2}\vec{E}_{tt}\cdot\vec{J}_s^{(2)}\,ds \qquad \text{(A-1)}$$

where the electric field can be replaced in terms of the dyadic Green's function $\overline{\overline{G}}(r,r')$ by

$$\vec{E}_{tt} = \iint_{\text{strip}} \overline{\overline{G}}(r,r')\cdot\vec{J}_t(r')\,ds'. \qquad \text{(A-2)}$$

By application of the reciprocity relation for the dyadic Green's function [22]

$$\overline{\overline{G}}(r,r')\cdot\vec{J}(r') = \vec{J}(r')\cdot\overline{\overline{G}}(r',r). \qquad \text{(A-3)}$$

(A-1) and (A-2) lead to

$$\iint_{\text{strip}} \vec{J}_t(r')\cdot\left[\iint_{\text{strip}}\overline{\overline{G}}(r',r)\cdot\vec{J}_e(r)\,ds + \iint_{S_1}\overline{\overline{G}}(r',r)\cdot\vec{J}_s^{(1)}(r)\,ds + \iint_{S_2}\overline{\overline{G}}(r',r)\cdot\vec{J}_s^{(2)}(r)\,ds\right]ds' = 0. \qquad \text{(A-4)}$$

Since the testing current $\vec{J}_t$ is arbitrary on the conducting strips, the expression inside the bracket of (A-4) has to vanish, which is the commonly used integral equation [19]. This signifies that total (tangential) electric field on the strips contributed by both the impressed sources ($\vec{J}_s^{(1)}$ and $\vec{J}_s^{(2)}$) and the induced current ($\vec{J}_e$) must be zero. The integral equation (A-4) is viewed as a result of the weighted residuals procedure with a testing (weighting) function of $\vec{J}_t$. When $\vec{J}_e$ is expanded by known basis functions, (A-4) leads to the method of moments, and to the Galerkin's method for $\vec{J}_t$ equal to the basis functions.

ACKNOWLEDGMENT

The authors are deeply grateful for the comments from two reviewers of this paper regarding the absolute convergence properties, number of modes and location of segmentation versus the strongly coupled subcircuits, surface waves, and many other details.

REFERENCES

[1] T. Okoshi, Y. Uehara, and T. Takeuchi, "The segmentation method: An approach to the analysis of microwave planar circuits," *IEEE Trans. Microwave Theory Tech.*, vol. MTT-24, pp. 662–668, Oct. 1976.
[2] R. Chadha and K. C. Gupta, "Segmentation method using impedance matrices for analysis of planar microwave planar circuits," *IEEE Trans. Microwave Theory Tech.*, vol. MTT-29, pp. 71–74, Jan. 1981.
[3] R. Sorrentino, "Planar circuits, waveguide models, and segmentation method," *IEEE Trans. Microwave Theory Tech.*, vol. MTT-33, pp. 1057–1066, Oct. 1985.
[4] F. Alessandri, M. Mongiardo, and R. Sorrentino, "Transverse segmentation: A novel technique for the efficient CAD of $2N$-port branch-guide couplers," *IEEE Microwave Guided Wave Lett.*, pp. 204–207, Aug. 1991.
[5] ——, "A technique for the fullwave automatic synthesis of waveguide components: Application to fixed phase shifters," *IEEE Trans. Microwave Theory Tech.*, vol. 40, pp. 1484–1495, July 1992.
[6] R. Sorrentino, F. Alessandri, M. Mongiardo, G. Avitabile, and L. Roselli, "Full-wave modeling of via hole grounds in microstrip by three-dimensional mode matching technique," *IEEE Trans. Microwave Theory Tech.*, vol. 40, pp. 2228–2234, Dec. 1992.
[7] F. Alessandri, G. Baini, M. Mongiardo, and R. Sorrentino, "A 3-D mode matching technique for the efficient analysis of coplanar MMIC discontinuities with finite metallization thickness," *IEEE Trans. Microwave Theory Tech.*, vol. 41, pp. 1625–1629, Sept. 1993.
[8] F. Alessandri, M. Mongiardo, and R. Sorrentino, "New efficient full wave optimization of microwave circuits by the adjoint network method," *IEEE Microwave Guided Wave Lett.*, vol. 3, pp. 414–416, Nov. 1993.
[9] F. Alessandri, M. Dionigi, and R. Sorrentino, "A fullwave CAD tool for waveguide components using a high speed direct optimizer," *IEEE Trans. Microwave Theory Tech.*, vol. 43, pp. 2046–2052, Sept. 1995.
[10] T. S. Chu and T. Itoh, "Generalized scattering matrix method for analysis of cascaded and offset microstrip step discontinuities," *IEEE Trans. Microwave Theory Tech.*, vol. MTT-34, pp. 280–284, Feb. 1986.
[11] Q. Xu, K. J. Webb, and R. Mittra, "Study of modal solution procedures for microstrip step discontinuities," *IEEE Trans. Microwave Theory Tech.*, vol. MTT-37, pp. 381–387, Feb. 1989.
[12] A. S. Omar and K. Schünemann, "Transmission matrix representation of finline discontinuities," *IEEE Trans. Microwave Theory Tech.*, vol. MTT-33, pp. 765–770, Sept. 1985.
[13] R. F. Harrington, *Time-Harmonic Electromagnetic Fields*. New York: McGraw-Hill, 1961, ch. 3.
[14] M. A. Saed, "A method of moments solution of a cylindrical cavity placed between two coaxial transmission lines," *IEEE Trans. Microwave Theory Tech.*, vol. 39, pp. 1712–1717, Oct. 1991.
[15] L. P. Dunleavy and P. B. Katehi, "A generalized method for analyzing shielded thin microstrip discontinuities," *IEEE Trans. Microwave Theory Tech.*, vol. 36, pp. 1758–1766, Dec. 1988.
[16] T. S. Horng, S. C. Wu, H. Y. Yang, and N. G. Alexopoulos, "A generalized method for distinguishing between radiation and surface-

wave losses in microstrip discontinuities," *IEEE Trans. Microwave Theory Tech.*, vol. 38, pp. 1800–1807, Dec. 1990.
[17] T. Becks and I. Wolff, "Analysis of 3-D metallization structures by a full-wave spectral domain technique," *IEEE Trans. Microwave Theory Tech.*, vol. 40, pp. 2219–2227, Dec. 1992.
[18] T. Tamir and A. A. Oliner, "Guided complex waves: Part I—Fields at an interface," *Proc. Inst. Elect. Eng.*, vol. 110, no. 2, pp. 310–324, Feb. 1963.
[19] W. Wertgen and R. H. Jansen, "Efficient direct and iterative electrodynamic analysis of geometrically complex MIC and MMIC structures," *Int. J. Numerical Modeling: Electron. Networks, Devices, and Fields*, vol. 2, pp. 153–186, Sept. 1989.
[20] K. J. Webb, P. W. Grounds, and R. Mittra, "Convergence in the spectral domain formulation of waveguide and scattering problems," *IEEE Trans. Antennas Propagat.*, vol. 38, pp. 869–877, June 1990.
[21] G. V. Eleftheriades, A. S. Omar, L. P. B. Katehi, and G. M. Rebeiz, "Some important properties of waveguide junction generalized scattering matrices in the context of the mode matching technique," *IEEE Trans. Microwave Theory Tech.*, vol. 42, pp. 1896–1903, Oct. 1994.
[22] R. E. Collin, *Field Theory of Guided Waves*. Piscataway, NJ: IEEE Press, 1991, ch. 2.

Shih-Ping Liu (S'96) was born in Taiwan, R.O.C., on December 8, 1965. He received the B.S. degree in engineering science from National Cheng Kung University, Tainan, Taiwan, R.O.C., in 1987. Since 1992, he has been working toward the Ph.D. degree at National Chiao Tung University, Hsinchu, Taiwan, R.O.C.

From July 1989 to August 1992, he was a Process Engineer and a Firmware Engineer. His current research interests include the analysis and design of microwave and millimeter-wave circuits.

Ching-Kuang C. Tzuang (S'80–M'86–SM'92) was born in Taiwan, R.O.C., on May 10, 1955. He received the B.S. degree in electronic engineering from National Chiao Tung University, Hsinchu, Taiwan, in 1977, the M.S. degree from the University of California at Los Angeles, in 1980, and the Ph.D. degree in electrical engineering from the University of Texas at Austin, in 1986, where he worked on high-speed transient analyses of monolithic microwave integrated circuits.

From February 1981 to June 1984, he was with TRW, Redondo Beach, CA, working on analog and digital monolithic microwave integrated circuits. Since September 1986, he has been with the Institute of Communication Engineering, National Chiao Tung University, Hsinchu, Taiwan, R.O.C. His research activities involve the design and development of millimeter-wave and microwave active and passive circuits, EM field theory, complex waves, and the design of various quasi-optical integrated antennas.